INTERNATIONAL JOURNAL FOR NUMERICAL METHODS IN FLUIDS
Int. J. Numer. Meth. Fluids 2005; **49**:905–931
Published online 29 July 2005 in Wiley InterScience (www.interscience.wiley.com). DOI: 10.1002/fld.1032

Multiple pressure variables methods for fluid flow at all Mach numbers

J. H. Park and C.-D. Munz*,†

Institut für Aerodynamik und Gasdynamik, Universität Stuttgart, Pfaffenwaldring 21, 70550 Stuttgart, Germany

SUMMARY

In this paper we present a method for the simulation of incompressible as well as compressible unsteady flows. At first we discuss three different forms, i.e. a primitive-, conservative- and a semi-conservative form of the governing equations. We use a semi-implicit time integration in such a fashion that the stability is guaranteed independently of the speed of sound and the resulting method is independent of the Mach number range. Moreover, with the application of the so-called multiple pressure variables (MPV) approach the difficulties with the pressure term can be circumvented as in the incompressible limit the hydrodynamic pressure decouples from the equation of state. Increasing approximation errors in the low Mach number regime are avoided. As a result, the proposed algorithm can also simulate incompressible flows as limit for zero Mach number. Copyright © 2005 John Wiley & Sons, Ltd.

KEY WORDS: MPV approach; fractional step; staggered grid

1. INTRODUCTION

From the historical point of view of computational fluid dynamics our algorithm for compressible and incompressible unsteady flows belongs to the so-called *pressure methods*. The classical projection method of Chorin [1] and the SIMPLE method of Patankar and Spalding [2], which were developed originally for incompressible flows, represent this class of methods. The extension of this approach for subsonic flows was first introduced by Casulli and Greenspan [3]. Their scheme uses the primitive form of the Navier–Stokes equations and is based on a space-staggered mesh. Only the terms which are related to the speed of sound are discretized implicitly. As a result, this method is unconditionally stable with respect to the CFL-condition for the speed of sound. This is too restrictive in the low Mach number

*Correspondence to: C.-D. Munz, Institut für Aerodynamik und Gasdynamik, Universität Stuttgart, Pfaffenwaldring 21, 70550 Stuttgart, Germany.
†E-mail: munz@iag.uni-stuttgart.de

Contract/grant sponsor: DFG

Received 21 January 2004
Revised 24 January 2005
Accepted 25 May 2005

regime for fully explicit methods, since the acoustic speed in this regime is much faster than the velocity of the flow.

Subsequently a similar approach in a conservative form called barely implicit correction for flux-corrected transport (BIC-FCT) algorithm was developed by Patnaik *et al.* [4]. They constructed a two stage algorithm using collocated variables. The first stage is an explicit predictor, which is implemented with positivity-preserving monotone FCT methods for the convective terms in order to calculate strong gradients or shock waves accurately. As an implicit corrector in the second stage the pressure correction equation, resulting from the coupling of the implicit terms in the momentum- and energy equation, is solved. Certainly this scheme produced better results for moderate and high Mach number flows. Recently a mixed form, in which a non-conservative form is used only for the energy equation, was introduced by Bijl and Wesseling [5] to achieve more efficiency in the pressure correction time stepping scheme. Hereafter we call it a semi-conservative form. For the temporal integration Wesseling *et al.* [6] applied Runge–Kutta time stepping schemes for the explicit convective terms. They solved the implicit pressure correction equation only once at each time step. van der Heul *et al.* [7] reformulated their scheme for the application to the conservation equations.

When the Mach number tends to zero, the compressible equations converge to their incompressible counterpart. The pressure waves become infinitely fast with respect to the fluid velocity and a sudden pressure equalization takes place. Hence, local gradients in the velocity field cannot generate large pressure gradients. Subsequently no large density gradient can occur. This incompressible limit is mathematically a rather subtle one, because the equations change their type: In the inviscid case from pure hyperbolic compressible equations to hyperbolic–elliptic due to the infinite propagation rates of the pressure waves. Using an asymptotic analysis the incompressible limit of a compressible flow has been considered by Klainerman and Majda [8, 9] for the isentropic case. Later Klein [10] extended the formal asymptotic considerations to the non-isentropic case. Based on these asymptotic considerations Munz *et al.* [11] proposed the multiple pressure variables (MPV) scheme for the low Mach number regime as extension of incompressible pressure correction methods. This scheme mimics the low Mach number limit behaviour in such a way that the numerical scheme survives this limit and coincide for $M = 0$ with a standard incompressible pressure correction method. The MPV scheme in Reference [11] has been formulated in primitive variables with application to the low Mach number regime. For the time-integration they used the Strang-splitting [12] method, that is only of first-order in time for the incompressible limit case.

In this paper we extend the multiple pressure variable idea as proposed in Reference [11] into two directions. First, it is shown that this approach may be applied to various forms of the basic equations of compressible fluid flow. In the low Mach number regime all the numerical schemes produce quite similar results. But, in the fully compressible regime the numerical results clearly show that shock waves are captured well, if the scheme is applied to the equations in conservation form. The combination of multiple pressure variables and conservative form establishes a numerical scheme that may be applied to fluid flow at all Mach numbers. The proposed version of the MPV approach may especially be applied to problems where in one region compressible and in another weakly compressible or even incompressible fluid flow occur. Because the first-order time approximation behaves well only for the simulation of steady problems, the method is extended to second-order accuracy in time to obtain the efficient solution of unsteady problems too. This second-order time-integration methods preserves the main structure of the MPV-method.

The outline of the paper is as follows. In Section 2 we introduce the dimensionless basic equations in three different forms with the application of the MPV ansatz, discuss their properties in the incompressible limit case and the methodology used. In Section 3 the semi-implicit time-integration is presented for the conservative form, whose stability condition is independent of Mach number. We explain briefly the spatial discretization in Section 4 and the high-order semi-implicit time-integration in Section 5. In Section 6 we show by numerical experiments, that only the conservative MPV fractional step method can solve high Mach number flows correctly, whereas for the low Mach number case the solutions obtained by all three forms of the basic equations converge to the correct solution and their solutions show nearly the same qualities. For these cases we also present the convergence rate of the high-order time-integration methods. The paper is closed by the conclusions.

2. GOVERNING EQUATIONS AND METHODOLOGY

2.1. Governing equations

The conservation equations for density ϱ, momentum per unit volume $\varrho\mathbf{u}$, and total energy per unit volume e in the compressible gas dynamics without consideration of viscosity and heat addition are

$$\begin{aligned} \frac{\partial \varrho}{\partial t} + \nabla \cdot (\varrho \mathbf{u}) &= 0 \\ \frac{\partial (\varrho \mathbf{u})}{\partial t} + \nabla \cdot [(\varrho \mathbf{u}) \circ \mathbf{u}] + \nabla p &= 0 \\ \frac{\partial e}{\partial t} + \nabla \cdot [(e + p)\mathbf{u}] &= 0 \end{aligned} \tag{1}$$

where the total energy density is

$$e = \varrho\varepsilon + \tfrac{1}{2}\varrho(\mathbf{u} \cdot \mathbf{u})$$

The equation of state relating the pressure to both the density and the specific internal energy ε, for an ideal gas, is taken to be

$$p = (\gamma - 1)\varrho\varepsilon$$

Using the following non-dimensional variables:

$$\varrho' = \frac{\varrho}{\varrho_0}, \quad \mathbf{u}' = \frac{\mathbf{u}}{|\mathbf{u}_0|}, \quad p' = \frac{p}{p_0}, \quad x' = \frac{x}{x_0}, \quad t' = \frac{t|\mathbf{u}_0|}{x_0}$$

where the subscript $(\cdot)_0$ denotes the reference values and the superscript $(\cdot)'$ indicates the quantities without dimension, a non-dimensionalized form of the equations is obtained

$$\frac{\partial \varrho'}{\partial t'} + \nabla \cdot (\varrho' \mathbf{u}') = 0$$

$$\frac{\partial(\varrho'\mathbf{u}')}{\partial t'} + \nabla\cdot[(\varrho'\mathbf{u}')\circ\mathbf{u}'] + \frac{1}{M^2}\nabla p' = 0$$

$$\frac{\partial}{\partial t'}\left[p' + (\gamma-1)M^2\,\frac{\varrho'(\mathbf{u}'\cdot\mathbf{u}')}{2}\right] + \nabla\cdot\left\{\left[\gamma p' + (\gamma-1)M^2\,\frac{\varrho'(\mathbf{u}'\cdot\mathbf{u}')}{2}\right]\mathbf{u}'\right\} = 0 \tag{2}$$

Here, M represents the global Mach number

$$M = \frac{|\mathbf{u}_0|}{\sqrt{p_0/\varrho_0}} = \frac{|\mathbf{u}_0|}{c_0} \tag{3}$$

which is a measure for the compressibility effect in the flow field. We defined the reference value of the sound velocity to be $\sqrt{p_0/\varrho_0}$ and avoided the factor γ to simplify the asymptotic considerations later. In the energy equation the total energy is splitted according to the energy relation and the equation of state that reads in the non-dimensionalized form as

$$e = \varrho\varepsilon + M^2\frac{1}{2}\varrho(\mathbf{u}\cdot\mathbf{u}) = \frac{p}{\gamma-1} + M^2\frac{1}{2}\varrho(\mathbf{u}\cdot\mathbf{u})$$

This form of the energy equation we will use within the numerical framework.

We note, that the global Mach number M appears in the equations, because we choose different characteristic values for the flow velocity $\mathbf{u}$ and sound speed c. This is necessary, because in the low Mach number regime the scales of the fluid and sound velocity spread. We emphasize that M is a global parameter characterizing the compressibility of the flow, while M_{loc} denotes the local flow Mach number.

The incompressible limit is obtained when the Mach number M tends to zero. The term $1/M^2$ before the pressure gradient in the momentum equation shows the singular behaviour of this limit. The maximal speed of the wave propagation in the non-dimensional equations amounts

$$\lambda'_{\max} = |\mathbf{u}'| + \frac{c'}{M} \tag{4}$$

Hence, in the limit $(M\to 0)$ the pressure waves get an infinite propagation rate and the compressible equations converge towards their incompressible counterparts. Within this limit the term ∇/M^2 has to be bounded. Insight into this mathematical and physical limit behaviour gives an asymptotic analysis shortly reviewed in the next subsection. From now on we omit the superscript $(\cdot)'$ in the non-dimensional equations.

If the solutions are continuously differentiable, the energy equation may be reformulated into a pressure equation

$$p_t + \mathbf{u}\cdot\nabla p + \gamma p\nabla\cdot\mathbf{u} = 0 \tag{5}$$

by the use of the mass and momentum equations.

2.2. Methodology

In the following we shortly review the asymptotic results of Klainerman and Majda [8] and Klein [10] to motivate our numerical approach. These authors proposed an asymptotic expansion for the physical variables in powers of the Mach number

$$\mathbf{w} = \mathbf{w}^{(0)} + M\mathbf{w}^{(1)} + M^2\mathbf{w}^{(2)} + \cdots \quad \text{with } \mathbf{w} = (\varrho, \mathbf{u}, p) \tag{6}$$

The asymptotic expansions are substituted into the non-dimensionalized equations. As usual the terms with the same powers of the Mach number are gathered and are separately set to zero. In the non-dimensionalized equations the gradient of the pressure is divided by the square of the Mach number. Hence, from the two leading order asymptotic equations of the velocity equation follows that the pressure gradient for the leading order terms $p^{(0)}$ and $p^{(1)}$ have to be zero as the Mach number tends to zero. The physical interpretation is the following. Due to the fact that the pressure waves become very fast, a sudden pressure equalization will take place. The result is that a local change in the velocity field cannot generate a strong pressure gradient and hence, the density does not change any more. The pressure becomes nearly constant, and splits into two main parts

$$p = p^{(0)} + M^2 p^{(2)} + O(M^2) \tag{7}$$

where both terms $p^{(0)}$ and $p^{(2)}$ survive the $M = 0$ limit and influence the leading order velocity term. The first-order pressure term $p^{(1)}$ is combined with the leading order term $p^{(0)}$ and named $p^{(0)}$ for simplicity, because it satisfies the same conditions, e.g. is constant in space. Because $p^{(0)}$ satisfies the equation of state it may be called the thermodynamic pressure that describes global background effects.

The time dependency of the pressure term $p^{(0)}$ is given from the leading order pressure Equation (5) that reads as

$$p_t^{(0)} + \gamma p^{(0)} \nabla \cdot \mathbf{u}^{(0)} = 0 \tag{8}$$

Here we used that the gradient of the thermodynamic pressure term is constant in space. Hence, the evolution equation for the background pressure is

$$-\frac{\mathrm{d}p^{(0)}}{\mathrm{d}t} = -\gamma p^{(0)} \nabla \cdot \mathbf{u} \tag{9}$$

The spatial averaging of the pressure equation (8) over the entire computational domain and applying the Gauss theorem leads to

$$\frac{\mathrm{d}p^{(0)}}{\mathrm{d}t} = -\frac{\gamma p^{(0)}}{|\Omega|} \int_{\partial\Omega} (\mathbf{u} \cdot \mathbf{n}) \, \mathrm{d}A \tag{10}$$

where $\mathbf{n}$ denotes the unit normal vector directed outward on the boundary $\partial\Omega$. This describes physically a global pressure change due to compression at the boundary. As a result we get the following divergence condition for the $M = 0$ limit:

$$\nabla \cdot \mathbf{u} = \frac{1}{|\Omega|} \int_{\partial\Omega} (\mathbf{u} \cdot \mathbf{n}) \, \mathrm{d}A \tag{11}$$

It is obvious, that the classical divergence-free condition of velocity ($\nabla \cdot \mathbf{u} = 0$) for incompressible flow can be retained, if no outer compression is active. Therefore, Equation (9) may be interpreted as a generalized divergence constraint in the $M = 0$ case, if outer compression occurs. Note that our divergence-free condition of velocity for incompressible flows in

this case does not result from the continuity equation, but from the pressure equation. The continuity equation reduces in this case simply to the transport equation for the density and becomes trivial, if the density is constant in space.

If we look for numerical methods that survive the limit $M=0$, the discretized equations should converge to the corresponding limit equations. Within the concept proposed we do not mean simply isochoric flow, but the flow of a compressible medium with infinite speed of sound. Hence, the numerical scheme may also be used to simulate zero Mach number variable density flows. Additionally, compression from the boundary are allowed, because the boundary conditions have not satisfied the incompressibility constraint. The limit equations for $M=0$ consists of the leading order mass equation, the leading order pressure equation (11) and the zeroth order momentum equation. The variables involved in the limit equations are $\varrho^{(0)}$, $\mathbf{u}^{(0)}$ and $p^{(2)}$. The second-order term $p^{(2)}$ acts as a balance-of-forces agent, which guarantees that the velocity satisfies the divergence constraint (11) for the velocity at $M=0$. Motivated by these asymptotic considerations Klein [10] denoted $p^{(0)}$ the thermodynamic pressure and $p^{(2)}$ the hydrodynamic pressure. More details on the asymptotic analysis and its physical meaning can be found in Reference [13].

In our construction of the numerical scheme we try to conserve this limit behaviour within the numerical framework. We introduce a splitting of the pressure according to (7) neglecting the higher order terms:

$$p = p^{(0)} + M^2 p^{(2)} \tag{12}$$

These multiple pressure variables are introduced into the equations of compressible fluid flow. They may be written in the following different forms:
Conservative form:

$$\begin{aligned}
&\frac{\partial \varrho}{\partial t} + \nabla\cdot(\varrho\mathbf{u}) = 0\\
&\frac{\partial(\varrho\mathbf{u})}{\partial t} + \nabla\cdot[(\varrho\mathbf{u})\circ\mathbf{u}] = -\nabla\cdot(p^{(2)}\mathbf{I})\\
&M^2\frac{\partial p^{(2)}}{\partial t} + \nabla\cdot(\gamma p\mathbf{u}) = -\frac{\mathrm{d}p^{(0)}}{\mathrm{d}t} - (\gamma-1)M^2\left[\frac{\partial e_k}{\partial t} + \nabla\cdot(e_k\mathbf{u})\right]
\end{aligned} \tag{13}$$

Semi-conservative form:

$$\begin{aligned}
&\frac{\partial \varrho}{\partial t} + \nabla\cdot(\varrho\mathbf{u}) = 0\\
&\frac{\partial(\varrho\mathbf{u})}{\partial t} + \nabla\cdot[(\varrho\mathbf{u})\circ\mathbf{u}] = -\nabla p^{(2)}\\
&M^2\frac{\partial p^{(2)}}{\partial t} + \nabla\cdot(p\mathbf{u}) + (\gamma-1)p\nabla\cdot\mathbf{u} = -\frac{\mathrm{d}p^{(0)}}{\mathrm{d}t}
\end{aligned} \tag{14}$$

Primitive form:

$$\begin{aligned} \frac{\partial \varrho}{\partial t} + \mathbf{u} \cdot \nabla \varrho &= -\varrho \nabla \cdot \mathbf{u} \\ \frac{\partial \mathbf{u}}{\partial t} + \mathbf{u} \cdot \nabla \mathbf{u} &= -\frac{\nabla p^{(2)}}{\varrho} \\ M^2 \frac{\partial p^{(2)}}{\partial t} + \mathbf{u} \cdot \nabla p &= -\gamma p \nabla \cdot \mathbf{u} - \frac{\mathrm{d}p^{(0)}}{\mathrm{d}t} \end{aligned} \tag{15}$$

Here, e_k is an abbreviation for the kinetic energy $\frac{1}{2}\varrho(\mathbf{u} \cdot \mathbf{u})$.

The aim of this reformulation of the equations is following. When the Mach number tends to zero, then all the three formulations converge formally to their incompressible counterparts. The terms multiplied by M^2 tends to zero and p tends to $p^{(0)}$ constant in space. If there is no compression from the boundary, the time derivative of $p^{(0)}$ becomes zero. The energy or pressure equation produces the divergence-free constraint for the fluid velocity. This reformulation of the non-dimensional equations gives the chance to construct a numerical method that formally converge to a method for the incompressible equations, when the Mach number tends to zero. On the other hand, the introduction of the multiple pressure variables does not change the equations. As long as the consistency relation (12) is valid the system with and without pressure splitting is equivalent for any positive Mach number. The introduction of multiple pressure variables is motivated by the low Mach number asymptotics and makes no sense for large Mach numbers. But, we did not introduce any approximation at that time and the equations are valid uniformly in M. We note that the different formulations of the compressible equations are equivalent only, if the solution is continuously differentiable.

In the numerical approximation we define initially the leading order pressure $p^{(0)}$ as average of p over the entire computational domain Ω

$$p^{(0)}(t) = \frac{1}{|\Omega|} \int_{\Omega} p \, \mathrm{d}\Omega \tag{16}$$

The time development of $p^{(0)}$ is calculated from Equation (10).

Within the numerical method proposed the pressure term $p^{(2)}$ is used as a primary variable. The pressure p is then obtained from Equation (12). The advantage is given within the low Mach number regime. The pressure $p^{(2)}$ converges formally to the hydrodynamic pressure satisfying the incompressible equations, while the pressure p becomes identical to the thermodynamic pressure $p^{(0)}$, if the Mach number tends to zero.

The construction principles for the numerical scheme are now the following. The stiffness of the equations for small Mach numbers is met by an implicit approximation, especially of those terms associated with the pressure waves. The other problem is the accuracy problem. Solving the equations for the pressure term p means that in the low Mach number regime the changes $O(M^2)$ have to been captured. This will introduce difficulties with respect to the accuracy and the increase of rounding errors. The direct solution of the pressure term $p^{(2)}$ instead of the p solves this accuracy problem. Having found $p^{(2)}$ this term is multiplied by M^2 and added according to (12). A similar rescaling for small Mach numbers has been introduced by Bijl and Wesseling [5]. They also define a hydrodynamic pressure term by subtracting a background pressure from the pressure term in the compressible equations and

introduce proper rescaling. The MPV approach makes the structure more obvious. In this approach the thermodynamic pressure is a solution of the equations itself. Hence, we can include variations of the thermodynamic pressure. We will outline these extensions to fluid flow with heat addition in the conclusions.

3. SEMI-IMPLICIT TEMPORAL DISCRETIZATION

For the fully explicit treatment of the above equations for $M \neq 0$ the stability of the numerical scheme can be guaranteed only under the following so-called CFL-condition:

$$\Delta t \leqslant \sigma \min_i \left[\frac{\Delta x}{|\mathbf{u}| + (c/M)} \right]_i \tag{17}$$

where $\sigma < 1$ is the so-called Courant number. This is often too restrictive for low Mach number flows. Casulli and Greenspan [3] have analysed the characteristic equations of the primitive system (15) and recognized that the speed of sound arises from the terms on the right-hand side of the velocity and the pressure equation. Hence, they discretized these derivative terms implicitly to obtain a numerical method being stable independently of the speed of sound and the global Mach number. We employ a similar semi-implicit method for the time-integration of the basic equations (13)–(15). Because all the convection terms will be treated explicitly we have a CFL-condition involving the fluid velocity

$$\Delta t \leqslant \sigma \min_i \left[\frac{\Delta x}{|\mathbf{u}|} \right]_i \tag{18}$$

For the approximation of unsteady solutions this is usually a natural condition for the accurate resolution of the problem.

In the following we apply first a discretization in time only. In this semi-discretization or method of lines approach the spatial derivatives in the governing equations are approximated by a spatial discretization method in the first step. From this a system of first-order ordinary differential equations is obtained. As an example we apply such an additive semi-implicit time-integration to the non-dimensional conservative equations (13)

$$\begin{pmatrix} \varrho \\ \varrho \mathbf{u} \\ M^2 p^{(2)} + (\gamma - 1) M^2 e_k \end{pmatrix}_t + \widetilde{\nabla} \cdot \begin{pmatrix} \varrho \mathbf{u} \\ (\varrho \mathbf{u}) \circ \mathbf{u} \\ (\gamma - 1) M^2 e_k \mathbf{u} \end{pmatrix}_{\text{ex}} + \widetilde{\nabla} \cdot \begin{pmatrix} 0 \\ p^{(2)} \mathbf{I} \\ \gamma p \mathbf{u} \end{pmatrix}_{\text{im}} = \begin{pmatrix} 0 \\ 0 \\ -p^{(0)}{}_t \end{pmatrix} \tag{19}$$

where $\widetilde{\nabla}$ means a finite difference operator in space. The subscript 'ex' and 'im' denote terms that are proposed to be approximated in an explicit or an implicit fashion, respectively. Here, we treat explicitly all the terms, which have no relation with the fast propagating pressure waves. The Jacobian matrix of the ex-flux has only the eigenvalues u in one space dimension. We use the conservative form as the basic system of equations, but use the hydrodynamic pressure $p^{(2)}$ as a basic variable in the numerical approximation.

Without introducing multiple pressure variables semi-implicit schemes in different formulations have been proposed by several authors. Based on the fully conservative equations (1) Patnaik *et al.* [4] solved for the conservative variables on a collocated grid. They discretized

implicitly the pressure term in the momentum equation and the velocity in the energy equation. Casulli and Greenspan [3] solved the system in primitive variables on a staggered grid arrangement, but treated explicitly all the pressure terms and implicitly only the divergence of velocity. With their characteristic analysis they proved that it does not effect the stability properties. In this case, the scheme is not strictly additive semi-implicit any more, but the coupling between the velocity and pressure becomes linear and simple. Otherwise one cannot avoid the expensive iterative solution process of a non-linear system of equations for the pressure. Munz *et al*. [11] proposed an iterative SIMPLE-type method based on the primitive variables and using multiple pressure variables. With a rescaling of the pressure for low Mach numbers Wesseling and his co-workers used all the three different formulations subsequently in the papers [5–7].

In the conservative formulation for the simplest EULER time-integration case we get the following fully discretized form:

$$\frac{\varrho^{n+1}-\varrho^{n}}{\Delta t}+[\widetilde{\nabla}\cdot(\varrho\mathbf{u})]^{n}=0$$

$$\frac{(\varrho\mathbf{u})^{n+1}-(\varrho\mathbf{u})^{n}}{\Delta t}+[\widetilde{\nabla}\cdot(\varrho\mathbf{u}\circ\mathbf{u})]^{n}=-\widetilde{\nabla}p^{(2)^{n+1}}$$

$$\frac{[M^2p^{(2)}+(\gamma-1)M^2e_k]^{n+1}-[M^2p^{(2)}+(\gamma-1)M^2e_k]^{n}}{\Delta t}$$

$$+(\gamma-1)M^2[\widetilde{\nabla}\cdot(e_k\mathbf{u})]^{n}=-\widetilde{\nabla}\cdot(\gamma p^{e}\mathbf{u}^{n+1})-\frac{p^{(0)^{n+1}}-p^{(0)^{n}}}{\Delta t}$$

The pressure p^e denotes the explicit approximation of the pressure p^{n+1} at the new time level. One can certainly use the linear extrapolation of the previous pressures. But choosing p^n as p^e is sufficient for the first-order time-integration case. The explicit density-, momentum- and kinetic energy flux terms due to the convection are denoted by C_ϱ, C_m and C_k. Rearranging the above equations, we get

$$\varrho^{n+1}=\varrho^{n}-\Delta t\cdot C_\varrho$$

$$(\varrho\mathbf{u})^{n+1}+\Delta t\widetilde{\nabla}p^{(2)^{n+1}}=(\varrho\mathbf{u})^{n}-\Delta t\cdot C_m$$

$$M^2p^{(2)^{n+1}}+\Delta t\widetilde{\nabla}\cdot(\gamma p^{e}\mathbf{u}^{n+1})=M^2p^{(2)^{n}}-\mathrm{d}\,p^{(0)^{n}}$$
$$-(\gamma-1)M^2[e_k^{n+1}-e_k^{n}+\Delta t\cdot C_k]$$

The solution procedure is now the following. At first the density is calculated using the continuity equation in a fully explicit manner. The velocity and pressure are obtained with a predictor–corrector algorithm similar to a fractional step or projection method [1, 14] for the incompressible case.

In the predictor step the tentative velocity $\mathbf{u}^*$ is evaluated using the momentum equation with the guessed pressure $p^{(2)^*}$. Then these tentative values are corrected in the corrector step to satisfy the pressure equation, too. Therefore the following corrector relations are defined:

$$\begin{aligned} \mathbf{u}^{n+1} &= \mathbf{u}^* + \delta\mathbf{u} \\ p^{(2)^{n+1}} &= p^{(2)^*} + \delta p^{(2)} \\ p^{n+1} &= p^{(0)^{n+1}} + M^2 p^{(2)^{n+1}} \\ &= p^{(0)^n} + \mathrm{d}p^{(0)^n} + M^2 p^{(2)^*} + M^2 \delta p^{(2)} \end{aligned} \tag{20}$$

where $\delta(\cdot)$ denotes the correction of the corresponding physical value. The temporal change of the thermodynamic pressure $\mathrm{d}p^{(0)^n}$ for the incompressible case acts as a predictor

$$\mathrm{d}p^{(0)^n} = -\frac{\Delta t \cdot \gamma p^{(0)^n}}{|\Omega|} \int_\Omega \mathbf{u}^n \cdot \mathbf{n}\, \mathrm{d}\Omega \tag{21}$$

From the momentum equation we obtain the relation between the velocity- and the pressure correction

$$\varrho^{n+1}\delta\mathbf{u} = -\Delta t \cdot \widetilde{\nabla}\delta p^{(2)} \tag{22}$$

To linearize the pressure equation, we evaluate explicitly the kinetic energy at the new time level with the tentative velocity ($e_k^* = \frac{1}{2}\varrho^{n+1}\mathbf{u}^* \cdot \mathbf{u}^*$)

$$\begin{aligned} M^2 p^{(2)^{n+1}} + \Delta t \widetilde{\nabla} \cdot (\gamma p^e \mathbf{u}^{n+1}) = M^2 p^{(2)^n} - \mathrm{d}p^{(0)^n} \\ - (\gamma - 1) M^2 [e_k^* - e_k^n + \Delta t C_k] \end{aligned} \tag{23}$$

This treatment is allowed in the low Mach number regime, because the error amounts only $O(M^2)$. In the higher Mach number case, the explicit treatment causes no problems, because in this regime the time steps should be chosen according to the sound velocity CFL-condition due to the accuracy reason in the unsteady case.

By substituting the ansatz (20) and the correction relation (22) into the pressure equation (23), we get the so-called pressure correction equation

$$\begin{aligned} M^2 \delta p^{(2)} - \Delta t^2 \widetilde{\nabla} \cdot \left[\frac{\gamma p^e}{\varrho^{n+1}} \widetilde{\nabla} \delta p^{(2)} \right] = M^2 [p^{(2)^n} - p^{(2)^*}] - \mathrm{d}p^{(0)^n} \\ - \Delta t \widetilde{\nabla} \cdot (\gamma p^e \mathbf{u}^*) - (\gamma - 1) M^2 \delta k^* \end{aligned} \tag{24}$$

with

$$\delta k^* = e_k^* - e_k^n + \Delta t C_k$$

For the incompressible limit case ($M = 0$) with constant density and without outer compression ($\mathrm{d}p^{(0)} = 0$), this reduces to the classical Poisson equation of the pressure correction $\delta p^{(2)}$. In

this case our corrector step is identical with a projection method for the incompressible case. Thus the proposed MPV fractional step method can be interpreted as an extension of the traditional incompressible projection (or fractional step) method to all Mach number flows.

In the actual simulation we decompose the total pressure p into two parts, i.e. the thermodynamic mean pressure $p^{(0)}$ and the hydrodynamic pressure $p^{(2)}$, but only once at the initial phase. Then at each time step we guess the temporal change of the thermodynamic mean pressure $\mathrm{d}p^{(0)^n}$ from Equation (21) and using the pressure correction equation (24) we get the hydrodynamic pressure $p^{(2)^{n+1}}$. But the mean value of the pressure $\overline{p^{(2)^{n+1}}}$ does not in general disappear, so it is favourable to update the pressure decomposition and correct the mean pressure $p^{(0)^{n+1}}$ at the end of each time step ($p^{(2)^{n+1}} \Leftarrow p^{(2)^{n+1}} - \overline{p^{(2)^{n+1}}}$, $p^{(0)^{n+1}} \Leftarrow p^{(0)^{n+1}} + M^2\overline{p^{(2)^{n+1}}}$). Otherwise the consistency between the different pressure terms is lost.

We briefly summarize our overall solution procedure:

1. At the initial phase the pressure must be decomposed according to the MPV ansatz (7).
2. At each time step first all the convective transport terms C_ϱ, C_m, C_k are calculated explicitly using the values at the old time level.
3. The density is calculated explicitly in time at the new time level.
4. The temporal change of the thermodynamic mean pressure $\mathrm{d}p^{(0)^n}$ is calculated according to (21).
5. A guess $p^{(2)^*}$ of the pressure is used to evaluate the tentative velocity $\mathbf{u}^*$ using the momentum equation.
6. The linearized pressure correction equation (24) is solved.
7. All the flow properties at the new time level $(\cdot)^{n+1}$ are evaluated according to relations (20).
8. For the compressible case the mean temporal change of $p^{(2)^{n+1}}$ must be subtracted from the incompressible pressure and added to the thermodynamic mean pressure $p^{(0)^{n+1}}$.
9. Go to the next time step.

For the primitive- and semi-conservative form we use a similar semi-implicit time-integration scheme and the same solution procedure. The differences lie in the pressure correction equations only. For the different approaches the following equations are obtained:
Pressure correction equation for the semi-conservative form

$$M^2\delta p^{(2)} - \Delta t^2\widetilde{\nabla}\cdot\left[\frac{p^e}{\varrho^{n+1}}\widetilde{\nabla}\delta p^{(2)}\right] - \Delta t^2(\gamma-1)p^e\widetilde{\nabla}\cdot\left[\frac{\widetilde{\nabla}\delta p^{(2)}}{\varrho^{n+1}}\right]$$
$$= M^2[p^{(2)^n} - p^{(2)^*}] - \mathrm{d}p^{(0)^n} - \Delta t\widetilde{\nabla}\cdot(p^e\mathbf{u}^*) - \Delta t(\gamma-1)p^e\widetilde{\nabla}\cdot\mathbf{u}^* \tag{25}$$

Pressure correction equation for the primitive form:

$$M^2\delta p^{(2)} - \Delta t^2\gamma p^e\widetilde{\nabla}\cdot\left[\frac{\widetilde{\nabla}\delta p^{(2)}}{\varrho^n}\right] = M^2[p^{(2)^n} - p^{(2)^*}] - \mathrm{d}p^{(0)^n}$$
$$- \Delta t\gamma p^e\widetilde{\nabla}\cdot\mathbf{u}^* \tag{26}$$

4. SPATIAL DISCRETIZATION

So far we considered the time approximation only and described the overall solution procedure. The approximation in space was not specified and several approximations may be applied. In the following we briefly discuss a simple spatial discretization based on a difference method. This approximation is based on a staggered grid arrangement, which was first introduced by Harlow and Welch [15] to compute incompressible flows. In this scheme scalar variables are defined at the cell centres, velocities at the cell boundaries. This is attractive for the incompressible flow, because a stable pressure–velocity coupling is established and no artificial terms are needed to avoid spurious pressure oscillations [16]. Whereas all the derivatives in the implicit part are approximated centrally, the convective transport terms in the explicit part are treated with upwind differences. As an example for upwinding, the density flux in ith cell is discretized by

$$\frac{1}{\Delta x}[(\varrho\mathbf{u})_{i+1/2} - (\varrho\mathbf{u})_{i-1/2}] \tag{27}$$

with

$$(\varrho\mathbf{u})_{i+1/2} = \mathbf{u}_{i+1/2} \cdot \begin{cases} \varrho_{i,+} & \text{for } \mathbf{u}_{i+1/2} > 0 \\ \varrho_{i+1,-} & \text{for } \mathbf{u}_{i+1/2} < 0 \end{cases} \tag{28}$$

Several methods for the left- $(+)$ or right $(-)$ interpolation of the density at the cell boundaries $i + \frac{1}{2}$ were developed in the last twenty years and are found in literature. Simply inserting ϱ_i for $\varrho_{i,+}$ and ϱ_{i+1} for $\varrho_{i+1,-}$ we can obtain only first-order in space. Using the piecewise linear interpolation, which originates from van Leer's MUSCL scheme [17], the second-order in space for smooth solutions is achieved

$$\varrho_{i,+} = \varrho_i + \frac{\Delta x}{2} S_{\varrho_i} \tag{29}$$

where S_{ϱ_i} represents the slope of density in ith grid zone. More details about the properties of this slope one can be found in Reference [18].

Because of the grid staggering we need additional interpolations for the density at cell boundaries in the momentum equation and the velocity at cell centres in the density- and pressure-transport terms. We use the second-order central interpolation for them

$$\varrho_{i+1/2} = 0.5(\varrho_i + \varrho_{i+1})$$

$$\mathbf{u}_i = 0.5(\mathbf{u}_{i-1/2} + \mathbf{u}_{i+1/2})$$

for the equidistant case. The spatially discretized pressure correction equation results in a linear algebraic system of equations for $\delta p^{(2)}$. This can be written as a simple tridiagonal system for the one-dimensional case and in general as a system with band matrix for the multi-dimensional case. For equidistant grids it is a symmetric system. As a solver we use CG-type methods with preconditioning.

5. SECOND-ORDER SEMI-IMPLICIT TIME-INTEGRATION

Up to now we have introduced only the simplest semi-implicit Euler method for the time-integration. For practical unsteady calculations second-order semi-implicit methods are necessary to increase the efficiency. The semi-discretization approach or method of lines leads to the first-order ordinary differential equations,

$$\frac{\mathrm{d}\Phi}{\mathrm{d}t} = \mathbf{f}(\Phi^n) + \mathbf{g}(\Phi^{n+1}) \tag{30}$$

where Φ is the vector of discretized flow field variables. Whereas $\mathbf{f}$ is the vector resulting from the spatial discretization of the non-stiff terms, $\mathbf{g}$ results from the stiff terms. Hence in the simulation $\mathbf{f}$ is approximated explicitly and $\mathbf{g}$ implicitly.

For such a strict additive semi-implicit time-integration, some one-step- and multistep methods with higher-order accuracy in time have been developed by several authors. Here we use the typical second-order methods, RK2CN- and SBDF method. In the following we apply these algorithms to our basic equations:

Euler method:

$$\Phi^{n+1} = \Phi^n + \Delta t[\mathbf{f}(\Phi^n) + \mathbf{g}(\Phi^{n+1})] \tag{31}$$

We have discussed this method in detail in the previous section. It is very simple, but we can achieve only first-order in time.

RK2CN method:

$$\begin{aligned} \Phi^{n+1/2} &= \Phi^n + \frac{\Delta t}{2}[\mathbf{f}(\Phi^n) + \mathbf{g}(\Phi^{n+1/2})] \\ \Phi^{n+1} &= \Phi^n + \Delta t\mathbf{f}(\Phi^{n+1/2}) + \Delta t[\tfrac{1}{2}\mathbf{g}(\Phi^n) + \tfrac{1}{2}\mathbf{g}(\Phi^{n+1})] \end{aligned} \tag{32}$$

The name RK2CN originates from the second-order Runge–Kutta method (midpoint rule) for the explicit term and the trapezoidal method (or Crank–Nicolson) for the implicit term. At the first stage flow variables at the half time-level are evaluated with the EULER method. Then these values are used for the explicit term at the second stage. For the implicit term the Crank–Nicolson scheme is applied. With this method we can achieve second-order in time. Unfortunately RK2CN method is only A-stable, but not strong A-stable (i.e. L-stable). With this method we observed difficulties with stability for nearly incompressible flows. In this regime one must treat the stiff terms fully implicitly.

SBDF method:

One of the most popular implicit multistep methods for stiff problems is the second-order backward differentiation formula (BDF) method, which is given, for the case of equidistant time steps, by

$$3\Phi^{n+1} - 4\Phi^n + \Phi^{n-1} = 2\Delta t[\mathbf{f}(\Phi^{n+1}) + \mathbf{g}(\Phi^{n+1})]$$

The SBDF (semi-implicit or extrapolated BDF) method is extended from the above classical two-step BDF method. For the non-stiff part one uses simple explicit linear extrapolation with time step ratio q

$$\mathbf{f}(\Phi^{n+1}) = (1+q)\mathbf{f}(\Phi^n) - q\mathbf{f}(\Phi^{n-1}), \quad q = \frac{t^{n+1}-t^n}{t^n - t^{n-1}}$$

Then we get the following SBDF2 formula:

$$\Phi^{n+1} = \frac{1}{1+2q}[(1+q)^2\Phi^n - q^2\Phi^{n-1}] + \frac{(1+q)\Delta t}{1+2q}[(1+q)\mathbf{f}(\Phi^n) - q\mathbf{f}(\Phi^{n-1}) + \mathbf{g}(\Phi^{n+1})] \tag{33}$$

The stability criteria for this method was analysed by Frank *et al*. [19].

Besides the above semi-implicit time-integration methods, some other second- or higher-order methods, i.e. ABCN method [20] as a two-step method or RK3CN- [21], UCS2- [22], ASIRK method [23] as a one-step method, are known in literature.

The splitting of the stiff and non-stiff terms into two subsystems leads to the problem of the definition of appropriate boundary values in both steps, especially in the non-physical intermediate step. We did not run into any difficulty for the problems numerically solved with the following procedure. All the terms that are explicitly approximated in the first step are connected with the fluid transport only and the corresponding system of evolution equations remains hyperbolic in the incompressible limit. To impose the boundary conditions we introduced dummy or fictitious grid cells. Appropriate values in the dummy grid cells are defined according to the physical situation and mathematical character of the equations. The initial data in the dummy grid cell are specified such that the proper values at the boundary are generated. We defined, e.g. for a fixed wall, the values in the dummy grid zones to be the same with respect to the interior domain for density, pressure, tangential velocity and anti-symmetric for the normal velocity component. This specification introduces a reflection of the convective motion at the wall. The technique used is quite common for the finite volume schemes. Here, the numerical flux at the boundaries is directly determined by the exact or approximate solution of these local initial value problems. In the second step all the physical boundary conditions are specified. Here, it is favourable to define the starting values of the pressure iteration for pressure and velocity such that they already satisfy the proper boundary conditions. Then for the pressure correction homogenous Dirichlet conditions may be prescribed.

6. NUMERICAL TESTS

The MPV-scheme for the basic equations in the primitive form was considered in Reference [16] using the implicit Euler method for time integration. There the well-known benchmark problem of the lid-driven cavity has been considered. The numerical results using the different formulations of the basic equations were almost the same. Hence, we will not show these results here. Differences between the results of the different formulations we would expect for larger Mach numbers, especially in the vicinity of shock waves.

The typical simple benchmark problems in the high Mach number regime are Riemann problems, for which exact solutions are available. In the solution of the Riemann problem shocks, contact discontinuities and expansion waves may occur. To simulate this flow structure correctly, numerical schemes must converge to weak solution. This means that an entropy condition must be satisfied, which rules out expansion shocks and that the numerical jump condition across the shock must be identical to the exact one. Otherwise the shock speed may be incorrect and may depend on the discretization parameters. For the time step condition we use the usual CFL-condition for an explicit method with the fixed Courant number $\sigma = 0.4$. For the solution of a Riemann problem this is a natural restriction for the accuracy. For the time-integration we apply the RK2CN method. As the slope parameter in the MUSCL scheme we choose $k = 1.0$, i.e. *minmod* function, because this slope calculation is quite robust and may suppress the oscillations at strong gradients. To validate the proposed methods in the low Mach number case we simulate the problem of two colliding pulses at the global Mach number $M \approx 0.1$ and the interaction of a density-layering with a long wavelength acoustic wave at $M \approx 0.02$. Here we use the time step condition (18) with respect to the flow velocity. For these test cases we also verify the convergence rates.

6.1. The shock tube problem of Sod

If the initial states are quiescent ($\mathbf{u}_l = \mathbf{u}_r = 0$), then the Riemann problem is also called a shock tube problem. The initial conditions for Sod's shock tube problem [24] are

$$M = 1; \ (\varrho_l, \mathbf{u}_l, p_l) = (1, 0, 1); \quad (\varrho_r, \mathbf{u}_r, p_r) = (0.125, 0, 0.1) \tag{34}$$

In the simulation we use 100 equidistant grid cells, $\Delta x = 0.01$. The maximal velocity in the flow amounts $|\mathbf{u}|_{\max} \approx 0.927$ and the maximal wave speed is $(|\mathbf{u}| + c)_{\max} = 2.2$.

In Figure 1 the density- , velocity-, pressure- and Mach number distributions for the three different forms of the basic equations are compared with the exact solutions. The results obtained from the primitive form are not acceptable. The shock speed is wrong and the constant values for the velocity and the pressure behind the shock wave clearly show deviations. For the semi-conservative formulation the results are much better. They are quite similar to those of the conservative formulation. They produce the proper shock speed and the overall deviation from the exact solution is small.

6.2. Test case of Lax

The initial state [25] is specified by

$$M = 1; \ (\varrho_l, \mathbf{u}_l, p_l) = (0.445, 0.698, 3.528); \quad (\varrho_r, \mathbf{u}_r, p_r) = (0.5, 0, 0.571) \tag{35}$$

As in the previous simulation we use 100 equidistant grid cells, $\Delta x = 0.02$. In this test case the shock and contact discontinuity are stronger than in Sod's shock tube problem. The maximal velocity in the flow amounts $|\mathbf{u}|_{\max} \approx 1.529$ and the maximal wave speed $(|\mathbf{u}| + c)_{\max} = 4.7$. As in the test case of Sod the results based on the primitive form are not acceptable, they show wrong constant states and wrong shock velocity. The results of the semi-conservative form and the conservative form now show stronger deviations. Especially the deviation in the density profile is quite obvious. The conservative form shows the correct behaviour (Figure 2).

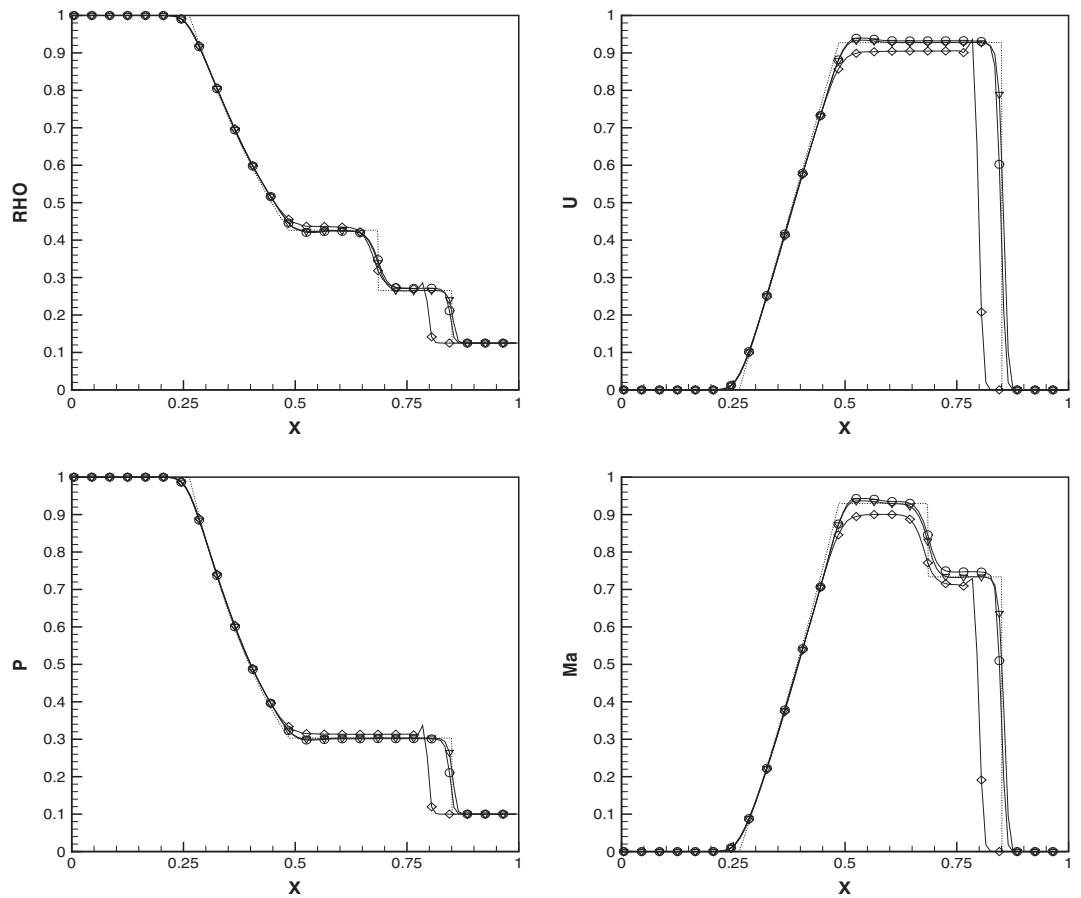

Figure 1. Sod's shock problem with at $t = 0.2$, $\diamond$: primitive form, ∇: conservative form, $\bigcirc$: semi-conservative form, dotted line: exact solution.

6.3. *The blast wave problem of Woodward–Collela*

This test case is the left half of the blast wave problem of Woodward and Collela [26], that is one of the severest test cases. Like in the previous test cases the solution consists of a left-running rarefaction wave and a right-running shock wave followed by a contact discontinuity. The initial conditions are given by

$$M = 1; \quad (\varrho_l, \mathbf{u}_l, p_l) = (1, 0, 1000); \quad (\varrho_r, \mathbf{u}_r, p_r) = (1, 0, 0.01) \tag{36}$$

We use 200 equidistant grid cells, $\Delta x = 0.01$. The maximal velocity in the flow amounts $|\mathbf{u}|_{\max} \approx 19.6$. Now the flow is supersonic in some region and the maximal Mach number reaches up to $M_{\text{loc}} \approx 1.89$. In this test case with such a strong pressure jump, the semi-conservative form shows its limits and produces non-reasonable results. As expected, for strong shock waves the conservative form of the governing equations is important to obtain good results. The numerical damping especially at the contact surface becomes clearly visible. For a better numerical resolution one needs finer grids.

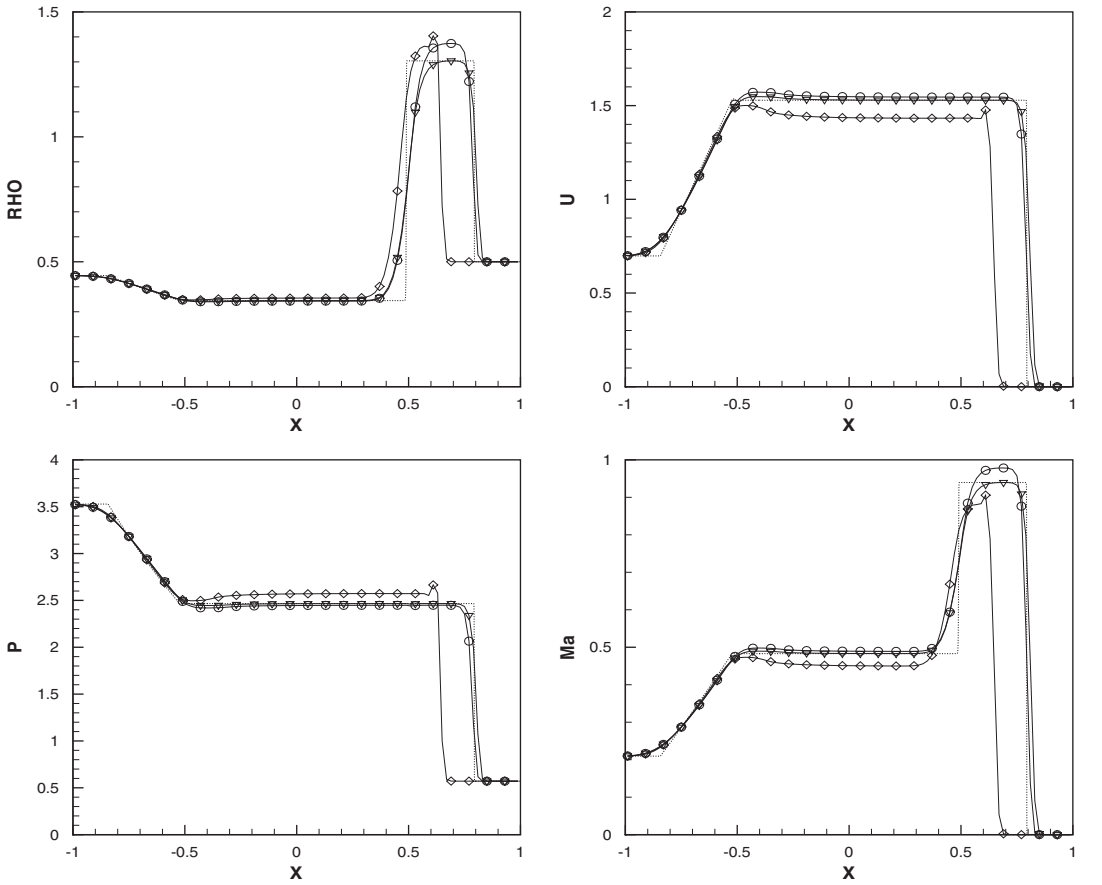

Figure 2. Lax's shock problem at $t = 0.32$, $\diamond$: primitive form, $\triangledown$: conservative form, $\bigcirc$: semi-conservative form, dotted line: exact solution.

The numerical results for the Riemann problem with moderate and strong shock waves indicate that the MPV-scheme based on the primitive variables is not able to capture a discontinuity in an appropriate way. The semi-conservative formulation produces still good results for moderate shock waves but run into trouble with the strong ones. In the case of strong discontinuities only the formulation in the conservative form produced acceptable results. The numerical experiments indicate that the shock speeds are reproduced very well. Due to the upwind differencing of the convection terms the scheme did not generate spurious oscillations at the discontinuities. Although the formulation of the numerical scheme is not the usual finite volume formulation by which the integral conservation property is automatically fulfilled, all the numerical results indicate that the use of the governing equations within our framework establishes the proper conditions at discontinuities. This is due to the fact that all the terms are approximated as fluxes on the staggered grid. The primary variables that are used in the pressure iteration is the pressure term $p^{(2)}$ and the velocity, but these variables are inserted into the fluxes of the conservative equations. The numerical dissipation introduced by the

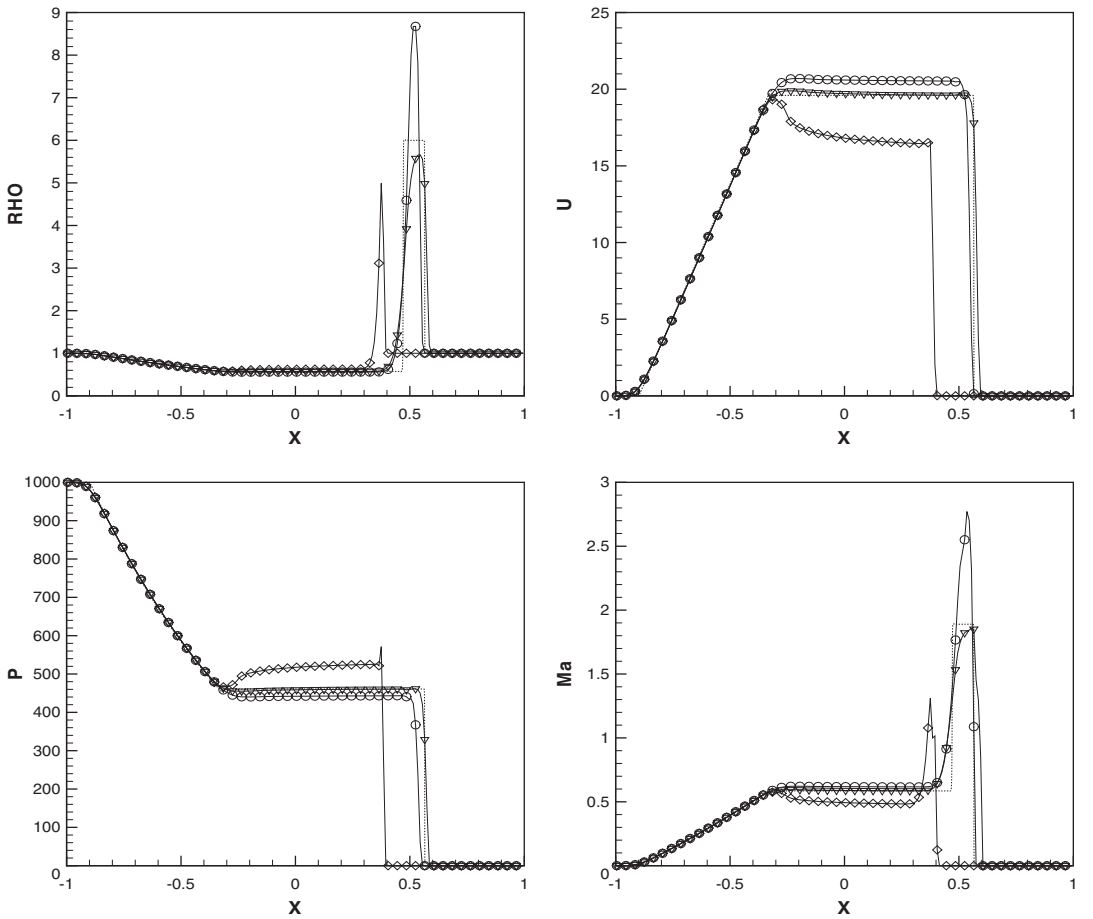

Figure 3. Woodward–Collela's problem with RK2CN method at $t = 0.024$, $\diamond$: primitive form, $\triangledown$: conservative form, $\bigcirc$: semi-conservative form, dotted line: exact solution.

upwind differencing of the convection terms, the central differencing of the pressure terms in combination with the implicit time approximation, and the averaging on the staggered grid seem to stabilize the calculation in such a way that the shock-capturing property is established (Figure 3).

6.4. *Two colliding pulses*

Next we show numerical results for the problem of two colliding pulses in a weak compressible regime ($M = \frac{1}{11}$). The initial data as proposed in Reference [10] are

$$\begin{aligned} \varrho(x,0) &= \bar{\varrho}_0 + M\tilde{\varrho}_0^{(1)} \cdot \tfrac{1}{2}(1.0 - \cos(2\pi x/L)) \\ p(x,0) &= \bar{p}_0 + M\tilde{p}_0^{(1)} \cdot \tfrac{1}{2}(1.0 - \cos(2\pi x/L)) \\ \mathbf{u}(x,0) &= \operatorname{sign}(x) \cdot \tilde{\mathbf{u}}_0 \cdot \tfrac{1}{2}(1.0 - \cos(2\pi x/L)) \end{aligned} \tag{37}$$

for $-L \leqslant x \leqslant L = \frac{2}{M}$, where

$$\bar{\varrho}_0 = 0.955, \quad \bar{p}_0 = 1.0$$

and

$$\tilde{\varrho}_0^{(1)} = 2.0, \quad \tilde{p}_0^{(1)} = 2\gamma, \quad \tilde{\mathbf{u}}_0 = 2\sqrt{\gamma}$$

These initial data generate two pulses, one right running pulse in $-L \leqslant x \leqslant 0$, and an antisymmetric left-running pulse in $0 \leqslant x \leqslant L$. We prescribe periodic boundary conditions and use 400 equidistant grid cells with $\Delta x = 0.1$. We choose the slope parameter in the MUSCL scheme $k = 1.4$, because no discontinuities exist in this a low Mach number regime. This problem was calculated by Klein [10] using a finite volume method modified for the low Mach number regime.

Figure 4 shows the pressure distribution at $t = 0.815$ and 1.63. The initial distribution is given as a dotted line. At $t = 0.815$ both pulses collide with each other and their superposition produces the maximal pressure. In the right figure both pulses separate again. Because of the weakly non-linear effects the front of the pulses steepens up considerably. The methods based on the three different forms show nearly identical results.

Now we test the convergence rate with different time step sizes with a fixed spatial grid. The time step size Δt is reduced successively with factor two ($\Delta t = \Delta x / 2^n$, $n = 2 \ldots 12$). We have no exact solutions for this test case, thus the solutions with the smallest time step size are taken as reference solution. With respect to these reference solution we evaluate the so-called normalized error [27]

$$\text{Normalized Error} = \frac{\sqrt{\Sigma |\Phi - \Phi_{\text{ref}}|^2}}{\sqrt{\Sigma |\Phi_{\text{ref}}|^2}} \tag{38}$$

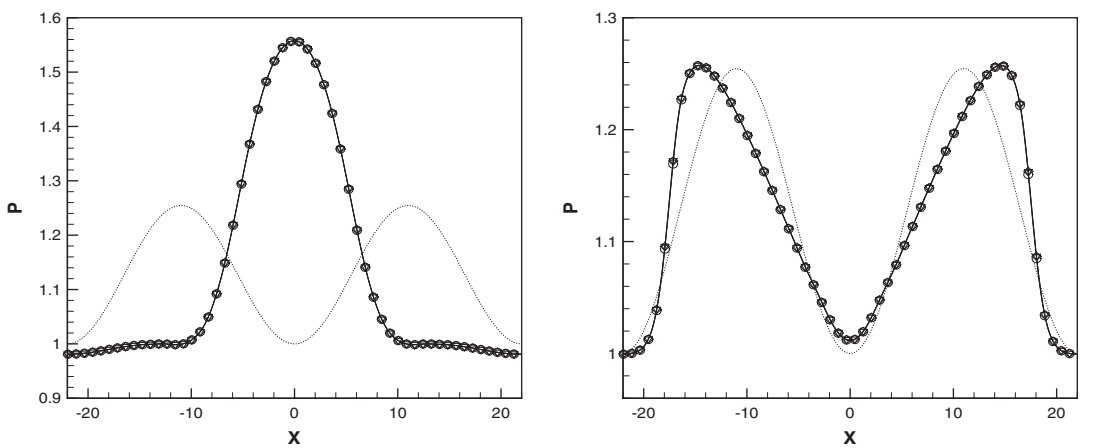

Figure 4. Pressure distribution of colliding acoustic pulses with RK2CN method at $t = 0.815$ (left), $t = 1.63$ (right), $\diamond$: primitive form, $\triangledown$: conservative form, $\bigcirc$: semi-conservative form, dotted lines: initial distribution.

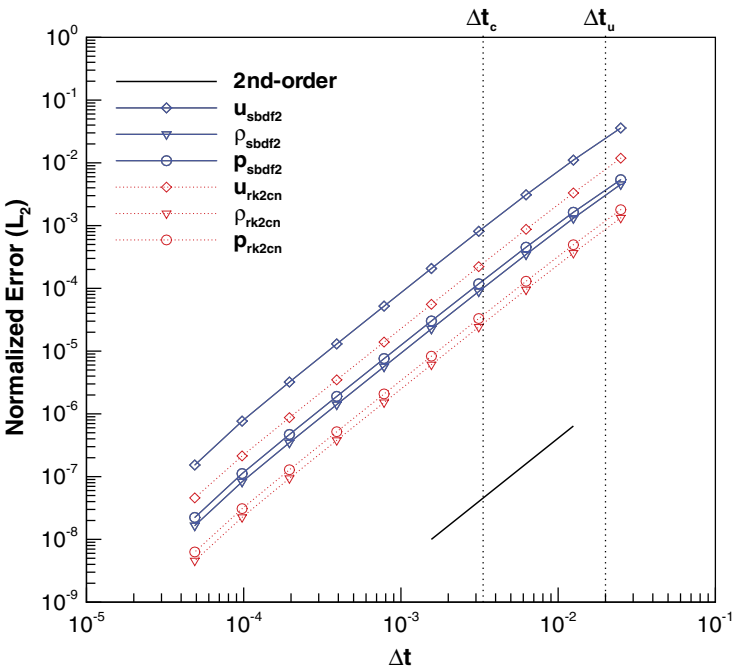

Figure 5. Convergence test of the colliding acoustic pulses at $t = 1.63$, $\diamond$: velocity, ∇: density, $\bigcirc$: pressure, solid lines: SBDF2 method, dotted lines: RK2CN method, thick line: slope of the second-order.

Figure 5 shows the results of the SBDF2- and RK2CN method with a logarithmic scale. Here, Δt_u is the maximal allowed time step size with respect to the CFL-condition for the flow velocity and Δt_c the time step size with respect to the normal CFL-condition for the speed of sound. Both methods achieve second-order in time for all variables and in all ranges. The error of the SBDF2 method is in general larger than that of the RK2CN method.

6.5. *Density-layering problem*

The initial data for this test case [10] are specified by

$$\begin{aligned} \varrho(x,0) &= \bar{\varrho}_0 + \Phi(x)\tilde{\varrho}_0^{(0)} \sin(40\pi x/L) + M\tilde{\varrho}_0^{(1)} \cdot 0.5 \cdot (1.0 + \cos(\pi x/L)) \\ p(x,0) &= \bar{p}_0 + M\tilde{p}_0^{(1)} \cdot 0.5 \cdot (1.0 + \cos(\pi x/L)) \\ \mathbf{u}(x,0) &= \tilde{\mathbf{u}}_0 \cdot 0.5 \cdot (1.0 + \cos(\pi x/L)) \end{aligned} \tag{39}$$

for $M = \frac{1}{51}$, $-L \leqslant x \leqslant L = 1/M$, with density coefficients

$$\bar{\varrho}_0 = 1.0, \quad \bar{p}_0 = 1.0$$

and the parameters

$$\tilde{\varrho}_0^{(1)} = 0.5, \quad \tilde{p}_0^{(1)} = 2\gamma, \quad \tilde{\mathbf{u}}_0 = 2\sqrt{\gamma}$$

The function $\Phi(x)$ is defined by

$$\Phi(x) = \begin{cases} 0 & -1/L \leqslant x \leqslant 0 \\ 0.5(1.0 - \cos(5\pi x/L)) & 0 \leqslant x \leqslant 2L/5 \\ 0 & x > 2L/5 \end{cases}$$

which smoothly limits the large amplitude short wavelength density fluctuations represented by $\tilde{\varrho}^{(0)}$. This test case operates with periodic boundary conditions too.

Above data represent a large amplitude, short wavelength density layering that is set in motion by a periodic train of long wavelength right-running pulses. The key aspect of this example is the advection of the density profile due to the recurring interaction with the background pulse. For this test case we choose a fine grid with 1020 grid points, i.e. $\Delta x = 0.1$ and the slope parameter $k = 1.4$ to resolve the small scale structures. Figure 6 shows the initial data in addition to the profiles at the later time $t = 5.071$ for the conservative form. By this time, the pressure pulse has passed the density layering two and a half times. Due to the weakly non-linearity of the pulse a considerable steepening of the pressure and velocity distribution is visible. The density fluctuation amplitude is preserved during the advection. The methods with other forms of the basic equations show the same quality in their solutions.

Similar to the previous test case we investigate the convergence rate. Figure 7 shows the results. There is a strong order reduction for all the solutions with the time step size between Δt_c and Δt_u. In this region the scheme can fully resolve the long wavelength right-running background pulse, but not sufficiently the acoustic perturbation waves, that arise due to interactions between the background pulse and the initial large amplitude short wavelength density fluctuations. Only after the complete resolution of these acoustic effects with time step size smaller than Δt_c, the proper convergence rate can be recovered again. Acoustic waves that appear in the weak compressible regime require sufficient small timesteps to capture their non-stationary behaviour.

6.6. *Vorticity generation in low Mach number flows*

This test case shows the vorticity generation in the low Mach number regime due to the interaction between the longwave acoustic pressure pulse and the small scale flow structures. Following initial data are given [28]:

$$\begin{aligned} \varrho(x, y, 0) &= \bar{\varrho}_0 + M\tilde{\varrho}_0^{(1)} \cdot 0.5 \cdot (1.0 + \cos(\pi x/L)) + \Phi(y) \\ p(x, y, 0) &= \bar{p}_0 + M\tilde{p}_0^{(1)} \cdot 0.5 \cdot (1.0 + \cos(\pi x/L)) \\ u(x, y, 0) &= \tilde{u}_0 \cdot 0.5 \cdot (1.0 + \cos(\pi x/L)) \\ v(x, y, 0) &= 0.0 \end{aligned} \tag{40}$$

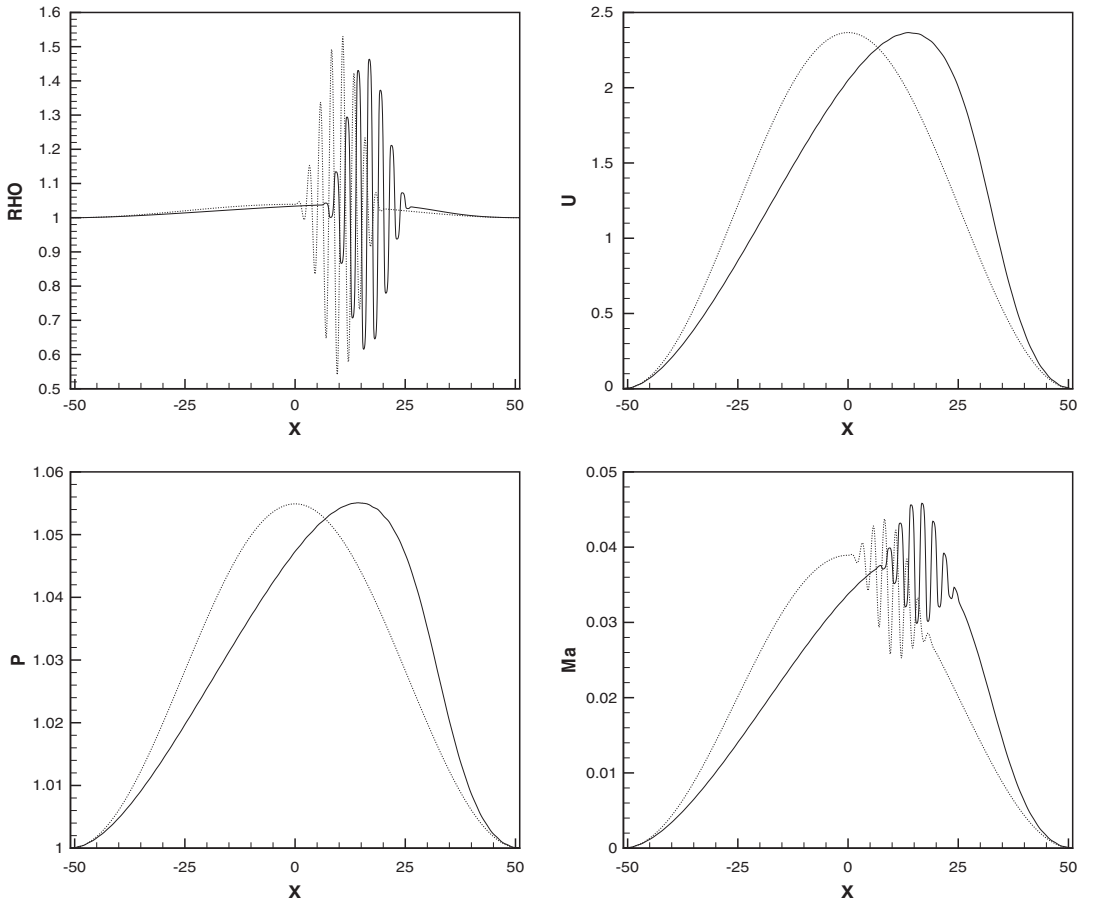

Figure 6. Density layering problem of Klein approximated with MPV-RK2CN method, dotted line: initial distributions; solid line: $t = 5.071$ for the conservative form.

for the Mach number $M = 0.05$ in the area $-L \leqslant x \leqslant L = 1/M$, $0 \leqslant y \leqslant L_y = 2L/5$ with the constant values

$$\bar{\varrho}_0 = 1.0, \quad \bar{p}_0 = 1.0$$

and

$$\tilde{\varrho}_0^{(1)} = 0.4, \quad \tilde{p}_0^{(1)} = 2\gamma, \quad \tilde{\mathbf{u}}_0 = 2\sqrt{\gamma}$$

The function $\Phi(y)$ is defined as

$$\Phi(y) = \begin{cases} 2\tilde{\varrho}_0^{(1)} \dfrac{y}{L_y}, & 0 \leqslant y \leqslant L_y/2 \\ 2\tilde{\varrho}_0^{(1)} \left(\dfrac{y}{L_y} - 1 \right), & L_y/2 \leqslant y \leqslant L_y \end{cases}$$

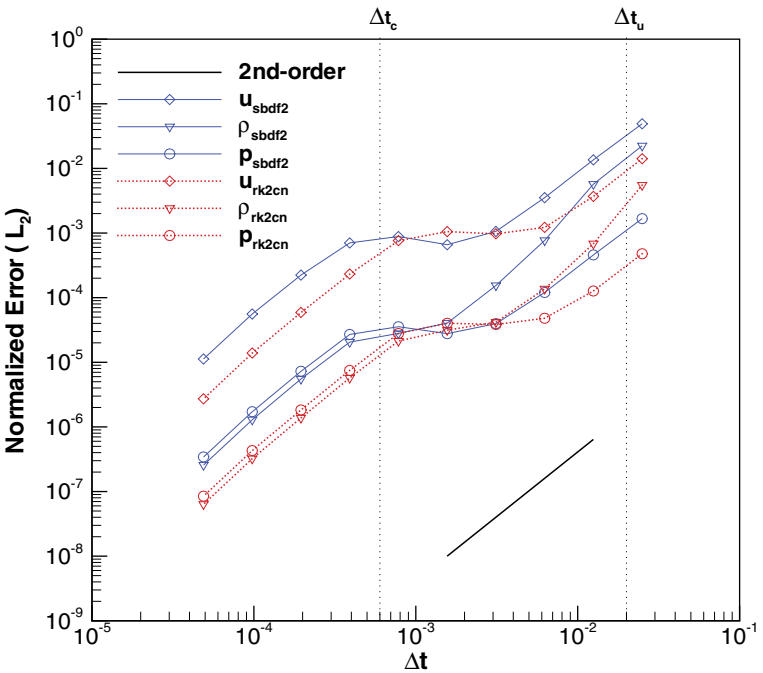

Figure 7. Convergence test of the density-layering problem at $t = 5.071$, $\diamond$: velocity, $\triangledown$: density, $\bigcirc$: pressure, solid lines: MPV-SBDF2 method, dotted lines: MPV-RK2CN method, thick line: slope of the second-order.

This represents a saw-tooth shaped density layering with the jump from $\varrho = 1.4$ to 0.6 in the y-direction. Our data describe a long wavelength periodic acoustic pulse with the amplitude γM, which runs over above the saw-tooth shaped density layering in the x-direction and sets it in motion. With the equidistant grid 400×80 the simulation was performed under the double periodic boundary conditions. We apply the SBDF2 method for the time-integration and MUSCL scheme with the slope parameter $\kappa = 1.4$.

At the initial state the flow is rotation-free. The fluid particles with different density near the interface are accelerated differently by the acoustic pressure pulse. Then the rotational motions arise slowly along the interface. These lead to the so-called Kelvin–Helmholtz instability. The long wavelength sinusoidal layer develops and continues to move in x-direction due to the driving long wavelength acoustic pulse. The sinusoidal density layer becomes itself unstable, especially on the flanks of the layer due to the strong density gradient. Then small rotational structures develop and grow very quickly. This example clearly demonstrates that the long wavelength acoustic pulse feed energy to the small space scale flow structures leading to the generation of vortices. Figure 8 shows the contour lines of density at the several developing phases of vortices. These results are obtained from the method based on the conservative form.

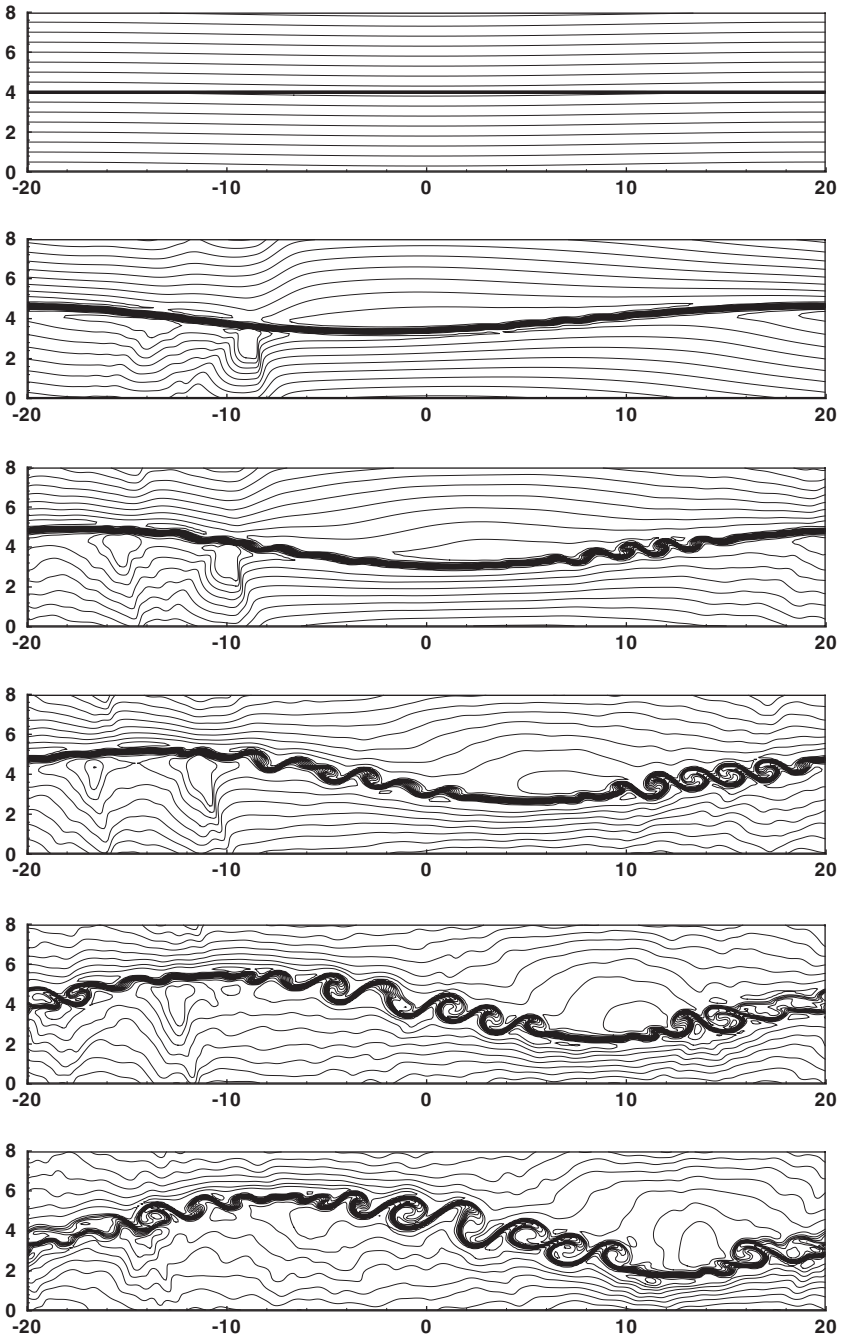

Figure 8. Vorticity generation due to the interaction between the long wavelength acoustic pressure pulse and the small scale flow structures at time $t = 0, 7, 10, 13, 16, 19$ for $M = 0.05$. Contourlines of the density: $= 0.65, 0.7, \ldots, 1.45$.

7. CONCLUSIONS

In this paper we investigated a pressure based method for the simulation of unsteady flows. The basic equations of compressible fluid dynamics are formulated in a primitive-, conservative- and semi-conservative form. The numerical method uses a staggered grid arrangement in space. As a time-integration we use a semi-implicit method, which treats only the acoustic terms implicitly, because the acoustic waves in the low Mach number regime are much faster than the flow velocity. Thus the stability condition of the overall algorithm is independent of the Mach number. Additionally we adopt the so-called MPV approach, which enables us to simulate compressible as well as incompressible flows. The decomposition of the pressure in a thermodynamic and a hydrodynamic part avoids the accuracy problems at low Mach numbers. As expected acceptable results for high Mach number flows are obtained only with the conservative form. For the low Mach number case the numerical solutions obtained by the primitive, semi-conservative and conservative forms of the basic equations converge to the correct solutions and their solutions show comparably the same qualities. The second-order semi-implicit time-integration methods is an important improvement to enhance the efficiency for unsteady problems.

Our conclusion is that the conservative MPV fractional step method, that is an extension of the incompressible projection (or fractional step) method, shows a good behaviour within the whole Mach number regime. The shock-capturing property is established by the use of the conservative equations. All the terms are approximated as numerical fluxes. The primary variables used in the pressure correction cycle are still the pressure and the velocity, but these values are inserted into the fluxes of the conservative formulation. The upwind differencing of the convection terms, the central differencing of the pressure terms in combination with the implicit time approximation, and the averaging on the staggered grid stabilize the scheme in the vicinity of discontinuities. The main fields of application of this technique are unsteady problems where in one region compressible and in another weakly compressible or even incompressible fluid flow occur. The version with the first-order time approximation behaves well for the simulation of steady problems. Looking for an unsteady solution of a problem in the fully compressible regime the implicit treatment is usually not necessary. Under such flow conditions an explicit finite volume shock-capturing scheme should need less computational effort. The explicit finite volume schemes run into the stiffness and accuracy problem within low Mach number regions. The so-called preconditioning methods that artificially reduce the speed of the acoustic waves may help to obtain stationary solutions. For unsteady problems a dual time-stepping has then to be introduced. Here, we expect that the MPV approach with the time accurate implicit treatment of the stiff terms will be more efficient.

All the results presented were for the inviscid equations. The extension to the Navier–Stokes equations is straightforward. The asymptotics may be extended to this case (see Reference [10]). The numerical scheme has then to be constructed in such a way that it converges to the $M = 0$ equations with heat conduction. In this case the evolution equation for the thermodynamic pressure contains the surface integral of the heat flux through the boundary. The thermodynamic background pressure may change in time. The other modification is that the heat conduction appears in the energy equation. The pressure correction equation becomes more complicated, because the heat flux depends on the temperature gradient that is determined by the caloric equation of state. This coupling has to be introduced into the iteration procedure. In the primitive formulation of the governing equations this has been

performed in Reference [11] and validated for the heat driven cavity with vertically heated walls. The temperature differences in this example were 150°, while the Mach number was still about 0.0005 with clear differences to results with the Boussinesq approximation.

ACKNOWLEDGEMENT

This work has been supported by the DFG.

REFERENCES

1. Chorin AJ. Numerical solution of the Navier–Stokes equation. *Mathematics of Computation* 1968; **22**:745–762.
2. Patankar S, Spalding S. A calculation procedure for heat, mass and momentum transfer in three dimensional parabolic flow. *International Journal of Heat and Mass Transfer* 1972; **15**:1787–1806.
3. Casulli V, Greenspan D. Pressure method for the numerical solution of transient, compressible fluid flows. *International Journal for Numerical Methods in Fluids* 1984; **4**:1001–1012.
4. Patnaik G, Guirguis RH, Boris JP, Oran ES. A barely implicit correction for flux-corrected transport. *Journal of Computational Physics* 1987; **71**:1–20.
5. Bijl H, Wesseling P. A unified method for computing incompressible and compressible flows in boundary-fitted coordinates. *Journal of Computational Physics* 1998; **141**:153–173.
6. Wesseling P, van der Heul DR, Vuik C. Unified methods for computing compressible and incompressible flows. *ECCOMAS*, 2000.
7. van der Heul DR, Vuik C, Wesseling P. A conservative pressure-correction method for flow at all speeds. *Computers and Fluids* 2003; **32**:1113–1132.
8. Klainerman S, Majda A. Singular limits of quasilinear hyperbolic systems with large parameters and the incompressible limit of compressible fluids. *Communications on Pure and Applied Mathematics* 1981; **34**: 481–524.
9. Klainerman S, Majda A. Compressible and incompressible fluids. *Communications on Pure and Applied Mathematics* 1982; **35**:629–653.
10. Klein R. Semi-implicit extension of a Godunov-type scheme based on low Mach number asymptotics I: one-dimensional flow. *Journal of Computational Physics* 1995; **121**:213–237.
11. Munz CD, Roller S, Klein R, Geratz KJ. The extension of incompressible flow solvers to the weakly compressible regime. *Computers and Fluids* 2002; **32**:173–196.
12. Strang G. On the construction and comparison of difference schemes. *SIAM Journal on Numerical Analysis* 1968; **5**:506–517.
13. Meister A. Asymptotic single and multiple scale expansions in the low Mach number limit. *SIAM Journal on Applied Mathematics* 1999; **60**:256–271.
14. Chorin AJ. On the convergence of discrete approximations to the Navier–Stokes equations. *Mathematics of Computation* 1969; **23**:341–353.
15. Harlow AT, Welch JE. Numerical calculation of time-dependent viscous incompressible flow of fluid with a free surface. *Physics of Fluids* 1965; **8**:2182–2189.
16. Patankar SV. *Numerical Heat Transfer and Fluid Flow*. Hemisphere Publishing: Washington, DC, 1980.
17. van Leer B. Toward the ultimate conservative difference scheme V: a second-order sequel to Godunov's method. *Journal of Computational Physics* 1979; **32**:101–136.
18. Sweby PK. High resolution schemes using flux limiter for hyperbolic conservation laws. *SIAM Journal on Numerical Analysis* 1984; **21**:217–235.
19. Frank J, Hundsdorfer W, Verwer JG. On the stability of implicit-explicit linear multistep methods. *Applied Numerical Mathematics* 1997; **25**:193–205.
20. Kim J, Moin P. Application of a fractional-step to incompressible Navier–Stokes equations. *Journal of Computational Physics* 1985; **59**:308–323.
21. Rai MM, Moin P. Direct simulations of turbulent flow using finite-difference schemes. *Journal of Computational Physics* 1991; **91**:15–53.
22. Liotta SF, Romano VR, Russo G. Central schemes for balance laws of relaxation type. *SIAM Journal on Numerical Analysis* 2000; **38**:1337–1356.
23. Zhong X. Additive semi-implicit Runge–Kutta methods for computing high-speed nonequilibrium reactive flows. *Journal of Computation Physics* 1996; **128**:19–31.
24. Sod GA. A survey of several finite difference methods for systems of non-linear conservation laws. *Journal of Computation Physics* 1978; **27**:1–31.
25. Lax PD. Weak solutions of non-linear hyperbolic equation and their numerical approximation. *Communications on Pure and Applied Mathematics* 1954; **7**:150–193.

26. Woodward P, Collela P. The numerical solution of two-dimensional fluid flow with strong shock. *Journal of Computational Physics* 1984; **54**:174–201.
27. Dukowicz JK, Dvinsky AS. Approximate factorization as a high order splitting for the implicit incompressible flow equations. *Journal of Computational Physics* 1992; **102**:336–347.
28. Geratz KJ. Erweiterung eines Godunov-Typ-Verfahrens für zwei-dimensionale kompressible Strömungen auf die Fälle kleiner und verschwindender Machzahl. *Ph.D. Thesis*, RWTH Aachen, 1997.

